Energies **2010**, *3*, 258-276; doi:10.3390/en3020258

OPEN ACCESS

energies
ISSN 1996-1073
www.mdpi.com/journal/energies

Article

The WRF Model Forecast-Derived Low-Level Wind Shear Climatology over the United States Great Plains

Brandon Storm [1] and Sukanta Basu [2,⋆]

[1] Wind Science and Engineering Research Center, Texas Tech University, Lubbock, TX, USA; E-Mail: Bstorm@eapc.net

[2] Atmospheric Science Group, Department of Geosciences, Texas Tech University, Lubbock, TX, USA

⋆ Author to whom correspondence should be addressed; E-Mail: sukanta.basu@ttu.edu.

Received: 15 January 2010 / Accepted: 20 February 2010 / Published: 23 February 2010

Abstract: For wind resource assessment projects, it is common practice to use a power-law relationship ($U(z) \sim z^{\alpha}$) and a fixed shear exponent ($\alpha = 1/7$) to extrapolate the observed wind speed from a low measurement level to high turbine hub-heights. However, recent studies using tall-tower observations have found that the annual average shear exponents at several locations over the United States Great Plains (USGP) are significantly higher than $1/7$. These findings highlight the critical need for detailed spatio-temporal characterizations of wind shear climatology over the USGP, where numerous large wind farms will be constructed in the foreseeable future. In this paper, a new generation numerical weather prediction model—the Weather Research and Forecasting (WRF) model, a fast and relatively inexpensive alternative to time-consuming and costly tall-tower projects, is utilized to determine whether it can reliably estimate the shear exponent and the magnitude of the directional shear at any arbitrary location over the USGP. Our results indicate that the WRF model qualitatively captures several low-level wind shear characteristics. However, there is definitely room for physics parameterization improvements for the WRF model to reliably represent the lower part of the atmospheric boundary layer.

Keywords: directional shear; low-level jet; numerical weather prediction; shear exponent

---

1. Introduction and Motivation

Wind energy in the recent years has become a valuable source of energy in the United States. As of 2008, nearly 21,000 MW capacity has been installed in the US, a majority of which is installed over the United States Great Plains (USGP), *i.e.*, central states such as Kansas and Texas [1]. Wind turbines commonly found in the USGP can have blades extending up to 150 m (Table 1) above ground level (AGL), with new turbines extending up to 200 m and higher. As shown in Figure 1, the modeled wind speed over the USGP exhibits a strong diurnal cycle, with large amounts of speed shear during the nighttime hours (*i.e.*, 0000–1200 UTC), due to the anti-phase relationship of the wind speeds near the surface and at higher heights. One reason for such behavior is a phenomenon referred to as low-level jet (LLJ). LLJs are wind maxima typically centered around 100 m to 1000 m AGL, which are frequently observed during nighttime hours in the USGP [2, 3, 4, 5]. Over the past 50 years, several physical mechanisms were proposed in the literature to explain the development and intrinsic characteristics of LLJs. They include (but not exclusively) inertial oscillations [6], baroclinicity generated by sloping terrain [7] and large-scale coupling [8].

Table 1. Characteristics of selected wind turbines commonly found in the USGP.

Turbine Manufacturer	Turbine Ratings (MW)	Diameter of Rotors (m)	Hub Height (m)	Max. Reach of Blades (m)
Mitsubishi	1	57–61.4	45–69	99.7
Suzlon	1.25	64–66	56–74	107
GE	1.5	70.5–77	61–100	138.5
Gamesa	2	80–90	60–100	145
Siemens	2.3	93	70–80	126.5
Vestas	3	90	80–105	150

Figure 1. The WRF model forecast-derived one-year (April 2006–March 2007) average diurnal wind speed variation at Sumner, KS. Left panel: diurnal cycle at different heights in the atmospheric boundary layer. Right panel: vertical profiles at specific times of the day.

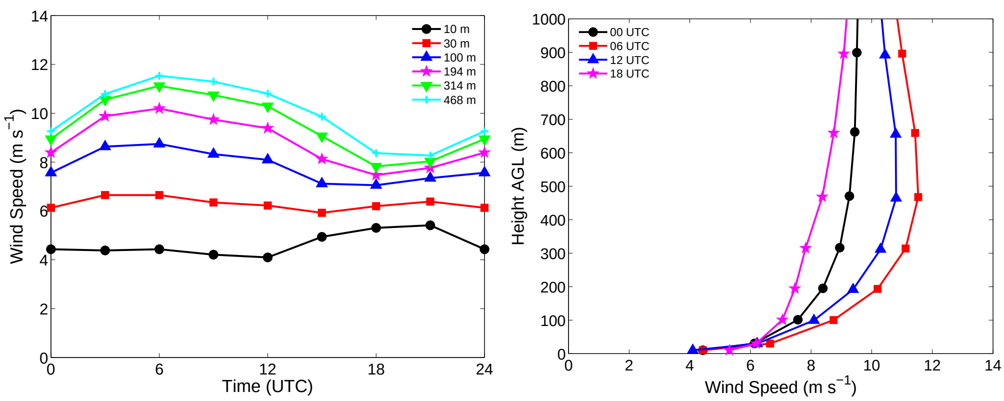

While LLJs and associated strong winds make the USGP a favorable location for wind power production, their presence can make it difficult to get an accurate estimate of turbine hub-height wind speeds. More importantly, the presence of LLJs can significantly modify the vertical wind shear and nighttime turbulence in the vicinity of the wind turbine hub height; thus, LLJs may have detrimental effects on rotors [9]. As modern-day utility-scale wind turbines are constructed in increasingly larger dimensions (higher hub-heights and larger rotor diameters), the impact of low-level wind shear will become more important, not just for wind power predictions, but for turbine load estimations as well.

The existing design codes (e.g., the International Electrotechnical Commissions Normal Turbulence Models [10]), which traditionally specify the inflow conditions for wind turbine designs, do not represent strong wind shear associated with nighttime boundary layers and LLJs. Thus, it is not surprising that suboptimal wind energy generation and turbine faults due to nighttime turbulence have been repeatedly reported in several USGP's wind farms [11, 12]. As an example, Figure 2 shows the seeming correlation between the wind turbine fault times and wind shear at Big Spring, Texas [13].

Figure 2. Diurnal variation of one-year average wind shear exponents (see Equation 1 for definition) along with turbine fault occurrences at Big Spring, TX. The observed average shear exponent values (black circles) and fault times (red squares) are reproduced from Smith *et al.* [13] using Engauge Digitizer 4.1. The WRF model forecast-based one-year average shear exponent values (black line with solid circles) have been calculated by the authors (see Section 3 for details).

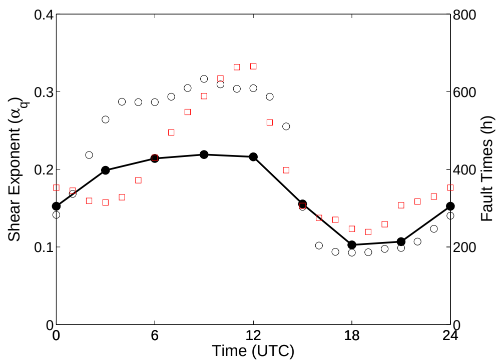

As with strong wind speed shear, wind directional shear (*i.e.*, the turning of wind with height) is also neglected in contemporary wind turbine design codes. During the daytime, wind directional shear is typically minimal within the entire boundary layer. However, during nighttime hours, average turning angles up to 40° (between 20 m and 200 m) have been reported in the literature [14]. Thus, it is very likely that the tall turbines in the USGP will suffer from large fatigue loads due to directional shear (see Giebel and Gryning [15] for similar speculations in the European context).

In summary, detailed spatio-temporal characterizations of wind speed and directional shears over the USGP are critical for the US wind energy industry. Reliable shear climatologies could be generated using a dense-network of tall-towers over the USGP. However, this is an expensive and virtually infeasible proposition. An alternative approach would be to use relatively inexpensive numerical weather prediction (NWP) model forecast-based shear climatologies. However, it is not known in the literature if the present-day NWP models are capable of reproducing wind speed shear and directional shear climatologies accurately. The present paper attempts to shed some light in this research arena. In this work, we generated high-resolution shear climatologies utilizing a state-of-the-art NWP model, known as the WRF model [16]. Wherever possible, we tried to highlight the strengths and weaknesses of the WRF model by comparing its results with available tall-tower observations. We also conducted sensitivity studies to understand the influences of different boundary layer parameterizations, as well as initial and boundary data on the modeled shear values.

The organization of this paper is as follows. In the following section, we briefly describe some concepts related to wind shear. In Section 3, both the numerically modeled and the observational data, as well as our shear computation approaches, are delineated. Comprehensive results are given in Section 4. Section 5 concludes this paper.

2. Wind Shear

To estimate wind speed at turbine hub-height, it is common practice to extrapolate the wind speed from a known height (usually 10 m) using the following power-law relationship:

$$U(z) = U_r \left(\frac{z}{z_r}\right)^{\alpha} \tag{1}$$

where U_r is the reference (or measured) wind speed at a given height, z_r, $U(z)$ is the estimated wind speed at height z, and α is the shear exponent. If a reference wind speed is known (from a nearby meteorological tower or an automated surface observing system—ASOS), the only unknown in Equation (1) is the shear exponent α. Note that Equation (1) is theoretically valid only for smooth pipe and laminar boundary layer flows (refer to [17] and the references therein for details). This equation does not have any sound theoretical basis for turbulent atmospheric boundary layers [18]. Nevertheless, Equation (1) enjoys a strong popularity in the wind energy community.

Over smooth terrains, the empirically estimated value of α is approximately $1/7$ or 0.14 under near-neutral atmospheric conditions (the regime where the buoyancy effects are virtually insignificant). Even though $\alpha = 1/7$ is commonly used for wind resource assessment projects, it is well-known that α strongly varies with atmospheric stability (intimately related to thermal stratification and shear generation), as well as surface roughness (e.g., Frost [19], Sisterson and Frenzen [20], and Irwin [21]). For this reason, recent studies have utilized tall-towers, typically communication towers, instrumented with anemometers to determine shear exponents at specific locations (e.g., Smith *et al.* [13], Schwartz and Elliot [22]). Most of these studies have found that large shear exponents exist during the nighttime hours, due to the increased atmospheric stability and, in some cases, also due to the presence of LLJs.

Some members of the wind energy community are beginning to acknowledge the fact that for most locations the average shear exponent is different from the widely assumed value of $1/7$. They are already using an average value of 0.2 for USGP's resource assessment projects. We would also like to point out that $\alpha = 0.2$ is "the standard" in wind turbine design codes [10]. A value of 0.2 for α may be appropriate for some locations, but due to the spatial and temporal variability of the shear exponent, this assumption could still be grossly inaccurate (overestimating at some locations and underestimating at others).

The wind directional shear is commonly estimated as: $\beta = D(z) - D(z_r)$, where $D(z)$ and $D(z_r)$ are wind turning angles at heights z and z_r, respectively. Due to strong turbulence mixing, the wind directional shear is quite minimal during the daytime. In contrast, during the nighttime, directional shear is typically large. Based on observational data from the Cabauw tower in the Netherlands, van Ulden and Holtslag [23] proposed the following empirical relationship for $D(z)$:

$$D(z)/D(h) = 1.58\,[1 - \exp(-z/h)] \tag{2}$$

where h is the boundary layer height and $D(h)$ is the wind turning angle at h. They estimated h by two diagnostic equations: one involving bulk Richardson number; other utilizing surface friction velocity, Obukhov length, and Coriolis parameter. They found that $D(h)$ is 35° for stably stratified (typically nighttime) cases.

3. Data and Methodology

3.1. Operational WRF Model Forecasts

To evaluate whether the WRF model [16] is accurately representing the wind shear climatology over the USGP, a year's worth of the WRF model (versions 2.1 and 2.2) forecasts was used to compute the wind speed shear exponents and the magnitudes of the directional shear. The WRF model forecasts were generated in real time by the National Center for Atmospheric Research (NCAR). Details of the operational WRF-NCAR model configuration can be found at: http://wrf-model.org/plots/wrfrealtime.php. Briefly, the physics parameterization options include: single-moment 3-class microphysics scheme [24], Rapid Radiative Transfer Model longwave radiation parameterization [25], Dudhia shortwave radiation scheme [26], Yonsei University planetary boundary layer (PBL) scheme [27], Noah land-surface model [28], and Kain-Fritsch cumulus parameterization [29, 30]. The operational WRF-NCAR model utilized a 36/12 km nested domain, 35 non-uniformly spaced vertical grid levels (7 levels were within the lowest 1 km), and was initialized from the Eta/NAM model forecasts at 0000 UTC every day. Forecasts were generated for 48 hours ahead with output stored every three hours. Only the 3-24 hour ahead forecasts were utilized in this study. During the study period (April 2006–March 2007), the WRF output was available for 337 days.

The lowest two vertical grid levels from the WRF model (approximately 30 and 100 m AGL) were used to calculate the wind speed shear exponent and directional shear magnitude across the USGP. Due to the terrain-following hydrostatic pressure vertical coordinate transformation in the WRF model, the model level heights slightly vary over the computational domain. Two different averaging methods, quenched and annealed, were used to determine the average shear exponents. The average shear exponent from the quenched method, α_q, calculates the shear exponent from every acceptable wind speed profile and then averages those values together, $\alpha_q \sim \left\langle ln\left(\frac{U_{100}}{U_{30}}\right)\right\rangle$. On the other hand, the annealed average shear exponent, α_a, uses the average wind speed at the appropriate levels to calculate the average shear exponent, $\alpha_a \sim ln\left(\frac{\langle U_{100}\rangle}{\langle U_{30}\rangle}\right)$. Here, the angular brackets denote temporal averaging. We would like to point out that the shear values were calculated only when the wind speeds at both heights (30 m and 100 m) were greater than 3 m s^{-1}. This particular threshold was chosen to reflect the fact that most of the utility-scale wind turbines' cut-in wind speed is on the order of 3 m s^{-1}.

Table 2. Specifications of different WRF model runs.

Model Run	WRF Version	Horizontal Grid Spacing (km)	Initial and Boundary Data	PBL Scheme	Output Frequency (h)
WRF-NCAR	2.1, 2.2	36/12	AWIP	YSU	3
WRF-YSU-NARR	3.1.1	27/9	NARR	YSU	1
WRF-MYJ-NARR	3.1.1	27/9	NARR	MYJ	1
WRF-QNSE-NARR	3.1.1	27/9	NARR	QNSE	1
WRF-ACM2-NARR	3.1.1	27/9	NARR	ACM2	1
WRF-YSU-NNRP	3.1.1	27/9	NNRP	YSU	1
WRF-YSU-FNL	3.1.1	27/9	FNL	YSU	1
WRF-YSU-AWIP	3.1.1	27/9	AWIP	YSU	1

3.2. Sensitivity Studies Using the WRF Model

In order to understand the influences of different PBL parameterizations, as well as initial and boundary data on the modeled shear values, we conducted sensitivity studies utilizing the most recent release of the WRF model (version 3.1.1). We simulated approximately two weeks period (May 19, 2006–May 31, 2006) with a 27/9 km nested domain ($\sim$ $2,000 \times 2,000$ km^2 outer domain, $\sim 675 \times 675$ km^2 inner domain) centered on Sweetwater, TX. This particular time period was selected because LLJs were forecasted almost every night near Sweetwater (see Figure 3) and thus episodes of high shear values were very likely. We used 51 non-uniformly spaced vertical grid levels (7 levels were within the lowest 1 km). In terms of physics parameterizations, we closely followed the WRF-NCAR specifications (see Section 3.1) with the exceptions of microphysics and PBL parameterizations. We utilized the mixed-phase 5-class microphysics scheme [24]. As shown in Table 2, a total of four different PBL schemes were utilized in the present study: Yonsei University scheme (YSU, [27]), Mellor-Yamada-Janjic scheme (MYJ, [31]), Quasi-Normal Scale Elimination scheme (QNSE, [32]), and Asymmetrical Convective Model version 2 scheme (ACM2, [33]). Four datasets with varying degree of spatial and temporal resolutions were utilized for initial and boundary conditions: North American Regional Reanalysis (NARR, 32 km resolution, every 3 hours), NCEP/NCAR Global Reanalysis Project (NNRP, 2.5 degree resolution, every 6 hours), NCEP GDAS FNL Analysis (FNL, 1 degree resolution, every 6 hours), and NCEP Eta/NAM (AWIP, 40 km resolution, every 6 hours). Following the strategy of the ARCMIP intercomparison study [34], all the simulations were run continuously throughout the entire two-week period without any data assimilation. In other words, during this simulation period, the model runs were only forced by the boundary conditions. WRF model forecasts were output and stored every hour. The wind shear values were computed following the procedures discussed in the previous sub-section.

Figure 3. Time-height plots of mean wind speed between May 19, 2006 and May 31, 2006. The panels represent (from top to bottom) WRF-NCAR, WRF-YSU-NARR, WRF-MYJ-NARR, and WRF-YSU-AWIP runs, respectively. Occurrences of low-level jets are clearly visible in all the model runs.

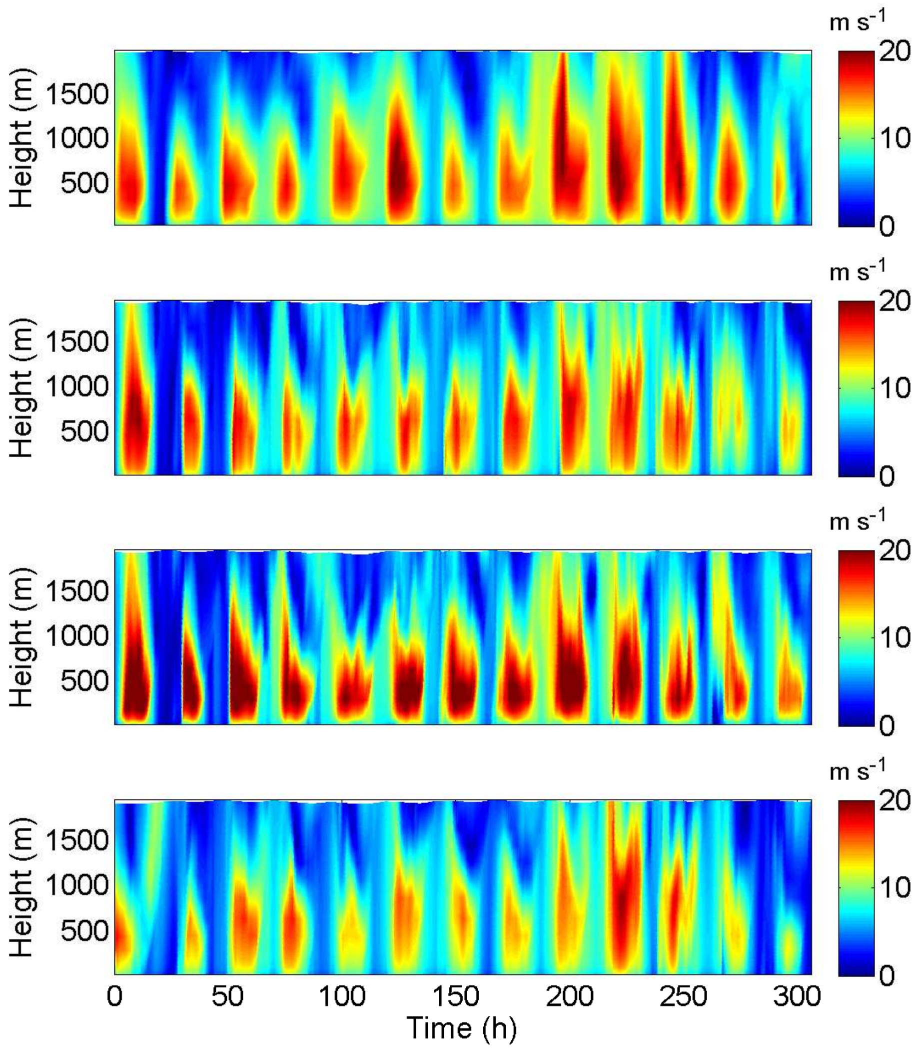

3.3. Observational Data

We utilized the wind data from a 100 m tall tower at Sweetwater, TX (maintained by the Alternative Energy Institute, www.windenergy.org) to validate the WRF model runs. On this tower wind speed values were measured at 50 m, 75 m, and 100 m levels. At each level two cup anemometers were installed, which enabled us to estimate the wind speed values reliably, as well as to compute the tower shadows. Wind directions were only measured at 50 m and 100 m levels. We estimated the wind shear values based on 50 m and 100 m data.

We further augmented our estimated wind shear values with the published values of Schwartz and Elliot [22] (henceforth SE06). SE06 utilized tall-tower observations over the USGP to calculate the annual average, as well as the diurnal cycle of α. They utilized several observational datasets of varying time periods (ranging from one to four years). Please note that SE06's study period does not include our study period of April 2006–March 2007. Furthermore, SE06 and the present study used quite different heights for the computations of α.

There are some technical and fundamental differences between the observations-based and the model forecast-derived wind shear estimations which need to be emphasized before discussing the results:

- Tall-tower observations are basically point measurements. In contrast, the WRF model forecast-derived statistics correspond to a spatial grid of 12 km (in the case of the operational WRF-NCAR run) or 9 km (in the case of the sensitivity study runs) resolution.
- While the WRF model forecasts represent instantaneous values (1 or 3 hourly), most of the observed wind speed values utilized by us and SE06 (personal communication, Elliot and Schwartz, 2007) were 10 minute averages.
- Data from the directional sectors affected by the tower structure (shadowing effects) were not considered by us and SE06. However, we analyzed all the directional sectors from the WRF model forecasts.

4. Results and Discussions

4.1. *Wind Characteristics at Sweetwater, TX*

Prior to determining the WRF model's ability to estimate site-specific shear exponents, it is worthwhile to first establish its capability to forecast the wind speed and direction values near turbine hub-height (around 100 m AGL) at a single location. For this purpose, one year (April 2006–March 2007) worth of the WRF-NCAR model forecast (from the grid point nearest to the tall-tower location) are compared with the wind data from the 100 m tall tower at Sweetwater. In Figure 4 the wind probability density functions (pdfs) based on these datasets are depicted. Various relevant wind statistics are reported in Table 3. The fitted Weibull probability density functions (red lines) are shown in Figure 4. The Weibull pdf is given by [35]:

$$f(U) = \frac{k}{c}\left(\frac{U}{c}\right)^{k-1} e^{-\left(\frac{U}{c}\right)^k} \tag{3}$$

where U is the wind speed, k is the Weibull shape factor, and c is the so-called scale factor. After fitting the Weibull pdfs, we estimated three insightful statistics [35]: (i) the most frequent wind speed $\left(U^F_{max} = c\left(\frac{k-1}{k}\right)^{1/k}\right)$, (ii) the wind speed contributing maximum energy $\left(U^E_{max} = \frac{c(k+2)^{1/k}}{k^{1/k}}\right)$, and (iii) the energy density $\left(E_D = \frac{\rho c^3}{2}\frac{3}{k}\Gamma\left(\frac{3}{k}\right)\right)$. From Figure 4 and Table 3 it is quite evident that the WRF-NCAR model forecast captured the characteristics of the observed wind at Sweetwater reasonably well. Specifically, we would like to highlight that the modeled energy density is within 4% of the observed value (note that for simplicity we assumed ρ to be equal to 1.2 kg m^{-3}).

Table 3. Comparison of the observed and the WRF-NCAR model forecast-derived wind speed related statistics at Sweetwater, TX (100 m AGL). Study period: April, 2006–March, 2007.

	$\overline{U}$ (m s^{-1})	c (m s^{-1})	k	U^F_{max} (m s^{-1})	U^E_{max} (m s^{-1})	E_D (W m^{-2})
Observation	8.36	9.42	2.56	7.76	11.80	544.09
WRF-NCAR	8.18	9.21	2.42	7.39	11.80	526.98

Figure 4. Comparison of the observed (left panel) and the WRF-NCAR model forecast-derived (right panel) wind speed probability density functions at Sweetwater, TX (100 m AGL). The red lines denote the fitted Weibull probability density functions. Study period: April, 2006–March, 2007.

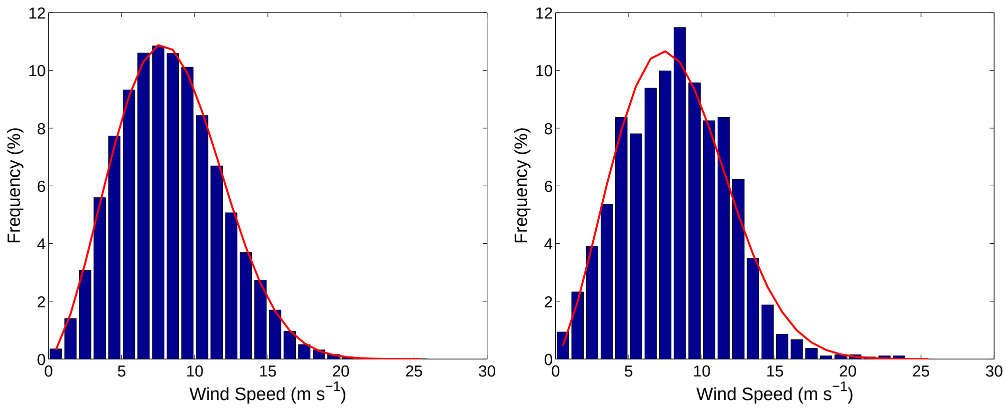

In Figure 5, wind roses are shown. At first glance, it might seem that the WRF-NCAR model forecast failed to correctly depict the wind direction at the 100 m level. The predominant modeled wind direction was (approximately) southerly, whereas the observed wind direction was more westerly. Given the discrepancy between the observed and the modeled wind direction at the 100 m level, we decided to compare these values with the observed wind direction at the 50 m level (bottom panel of Figure 5). Interestingly, at the 50 m level, the observed wind was predominantly southerly (top panel of Figure 5). The excessive difference between the 50 m and 100 m observed wind directions cannot be physically explained and is likely due to instrument error at the 100 m level. For this reason, we decided not to compute the wind directional shear values from the observed dataset.

In Table 4, various statistics related to the observed and the WRF-NCAR model forecast-derived annual average shear exponents and directional shear magnitudes at Sweetwater, TX are reported. Without any doubt the model represented the wind speed shear exponents (both α_q and α_a) very accurately. The standard deviation of the wind speed shear exponents (σ_{α_q}) are higher in the case of the observed data in comparison with the modeled data. This is to be expected as the observed data were available every 10 minutes and the modeled data had an output frequency of 3 hours. In this table, β_q and σ_{β_q} denote the mean and the standard deviation of the wind directional shear (quenched averaging was employed), respectively. Since we could not estimate the observed directional shear information due to likely sensor issues, we cannot provide direct validation of the WRF-NCAR model's results.

Figure 5. Comparison of the observed (top-left panel) and the WRF-NCAR model forecast-derived (top-right panel) wind roses at Sweetwater, TX (100 m AGL). The observed wind rose at 50 m AGL is also shown (bottom panel). Study period: April, 2006–March, 2007.

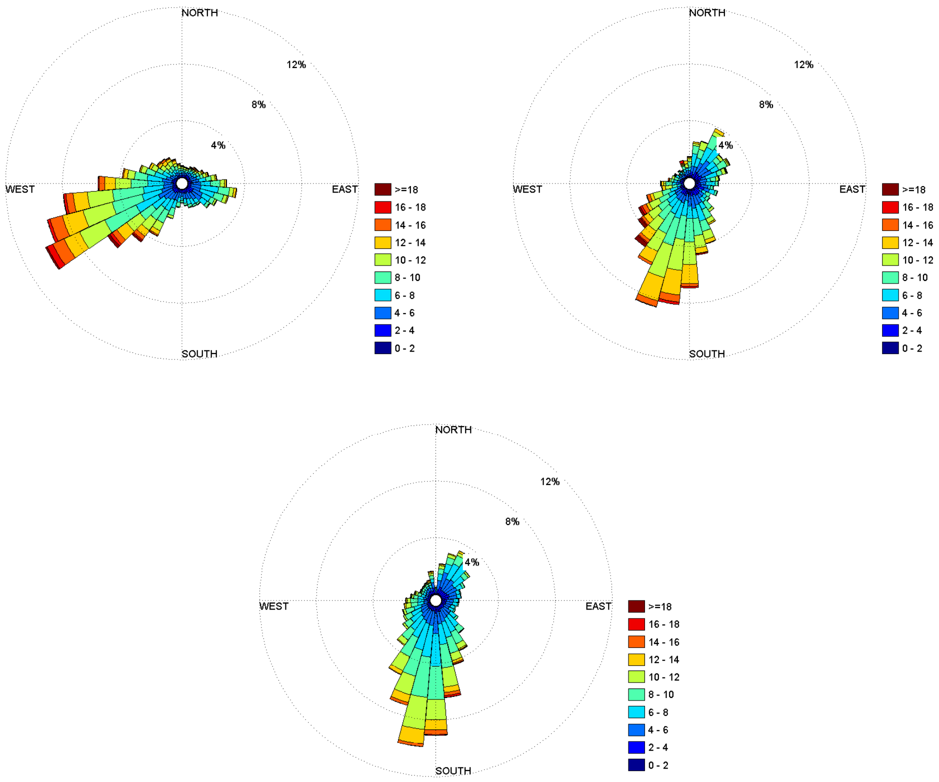

Table 4. Means and standard deviations of the observed and the WRF-NCAR model forecast-derived annual average shear exponents and directional shear magnitudes at Sweetwater, TX. Study period: April, 2006 – March, 2007.

Anemometer Heights (m)	Observed α_q	Observed σ_{α_q}	Observed α_a	WRF Grid Levels (m)	WRF α_q	WRF σ_{α_q}	WRF $\beta_q(^\circ)$	WRF $\sigma_{\beta_q}(^\circ)$	WRF α_a
50, 100	0.169	0.136	0.182	30, 101	0.168	0.072	2.22	3.42	0.177

The shear exponents show strong diurnal cycles (Figure 6). The WRF-NCAR model forecasts overestimated the shear exponents during the daytime hours (*i.e.*, 1500–2300 UTC), and underestimated the shear exponents during the nighttime hours. The nighttime underestimations are likely related to the "enhanced mixing" of the PBL schemes. It is worth mentioning that most of the present-day NWP models use PBL parameterizations, which are not physically based but "inspired by model performance" [36, 37]. Some of these ad-hoc parameterizations alleviate problems, such as "runaway-cooling", by (artificial) enhanced mixing. At the same time, these "fixes" create unphysical consequences, such as unreasonably deep boundary layers [37, 38] and weaker LLJs. At this point, we are unable to offer any physical explanation for the presence of excessive shear in the WRF model's daytime forecasts.

Figure 6. Diurnal variation of the observed and the WRF-NCAR model forecast-derived annual average wind shear exponents (left panel) and the directional shear magnitudes (right panel) at Sweetwater, TX. Study period: April 2006–March 2007.

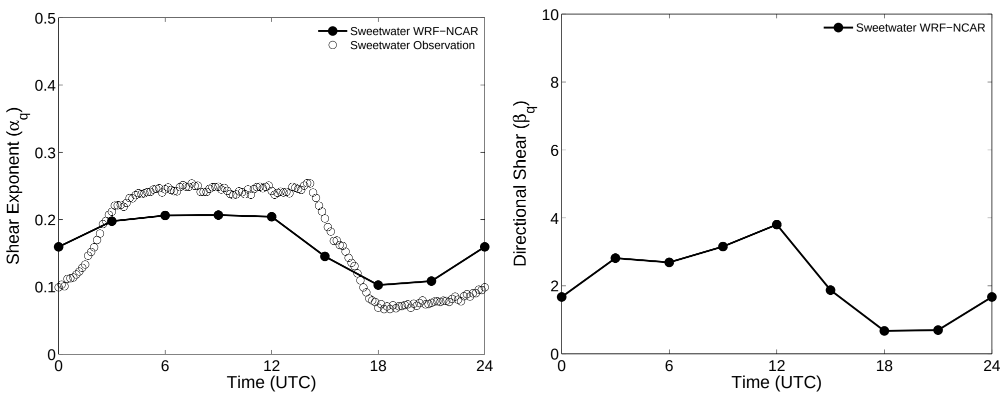

4.2. *Wind Shear Values at a Few USGP Sites*

To further ascertain whether the WRF model can be used to reliably determine site-specific shear exponents, in this sub-section the WRF-NCAR model forecast-derived one-year average shear exponents were compared with the published results of SE06. First of all, for almost all the locations, the observed as well as the WRF model forecasted α values were much larger than $1/7$. However, in contrast to the observations, the WRF-NCAR model underestimated the shear exponents (*i.e.*, $\alpha_q < \alpha$) at 7 out of 11 locations investigated. The maximum underestimation being $\sim$ 30% at Sumner, KS. On the other hand, the maximum overestimation is $\sim$ 24% at Kearny, KS. It should be noted that SE06 questioned the validity of the wind data from Kearny due to possible tower effects. Of course, tower shadowing and other measurement issues are never present in any numerical modeling approach (such as the WRF model).

The over- and under-estimation of the WRF-NCAR model forecast-derived wind speed shear exponents could also be (partially) attributed to the inter-annual variability of these exponents. We would like to remind the readers that SE06 utilized several observational datasets of varying time periods (ranging from one to four years). In contrast, we used one year worth of observed and modeled wind data (April 2006–March 2007). For Sweetwater, TX SE06 used wind data from May 17, 2003 to March 2, 2005. Tables 4 and 5 clearly show that, in comparison to SE06, our estimated observed wind speed shear exponent values were in much better agreement with the WRF-NCAR model forecast-derived values.

Table 5. Various statistics related to the observed and the WRF-NCAR model forecast-derived average shear exponents and directional shear magnitudes. Study period: varying time periods for the observed data and April 2006–March 2007 for the WRF-NCAR model forecasts.

Site Name	Anemometer Heights (m)	Observed α	WRF Grid Levels (m)	WRF α_q	WRF σ_{α_q}	WRF $\beta_q(^\circ)$	WRF $\sigma_{\beta_q}(^\circ)$	WRF α_a
Elk City, OK	40, 70	0.227	30, 101	0.174	0.076	2.51	3.48	0.180
Ellsworth, KS	50, 110	0.165	30, 100	0.178	0.077	2.99	3.76	0.185
Hobart, OK	40, 70	0.195	30, 101	0.175	0.076	2.58	3.66	0.182
Jewell, KS	50, 110	0.206	30, 99	0.175	0.073	2.93	3.71	0.180
Kearny, KS	50, 80	0.138	30, 99	0.171	0.078	3.34	4.11	0.176
Lamar, CO	52, 113	0.150	29, 98	0.152	0.086	4.11	5.18	0.163
Logan, KS	50, 80	0.179	30, 99	0.172	0.080	3.02	3.86	0.179
Ness, KS	50, 110	0.223	30, 100	0.172	0.078	3.00	3.79	0.178
Sumner, KS	50, 80	0.254	30, 100	0.177	0.078	3.04	3.79	0.182
Sweetwater, TX	50, 100	0.220	30, 101	0.168	0.072	2.22	3.42	0.177
Washburn, TX	50, 75	0.170	30, 100	0.172	0.075	2.61	3.47	0.180

The α_a values were marginally (less than 10%) higher than α_q at all the locations. This indicates that a rough estimation of the annual average shear exponent could be established if average wind speeds are known at various levels.

Table 5 portrays that there is a large spread of the shear exponents, which can be partially accounted for by the strong diurnal cycle in the shear exponents (Figure 7). SE06 reported diurnal cycles for 3 locations: Sumner, KS; Washburn, TX; and Lamar, CO. For all these locations, the WRF-NCAR model forecasts overestimated the shear exponents during the daytime hours, and underestimated the shear exponents during the nighttime hours. These results are in agreement with those reported for Sweetwater, TX in the previous sub-section.

The WRF-NCAR model forecast-derived directional shear magnitudes for the 11 USGP sites are also reported in Table 5. Since, SE06 did not document any observed directional shear information, we cannot provide direct validation of the WRF model's results. However, there is enough turning observed in the WRF model to highlight that the wind turbine design codes should take directional shear into consideration in the near future. A strong diurnal cycle was also observed for the magnitude of the directional shear (Figure 7), with large turning observed during the nighttime hours. We propose that directional shear magnitudes from the USGP towers be gathered and compared to the WRF model forecast-derived values before any credence is placed on these results.

Figure 7. Diurnal variation of the observed and the WRF-NCAR model forecast-derived annual average wind shear exponents (left panel) and the directional shear magnitudes (right panel). Observed shear exponents are reproduced from SE06 using Engauge Digitizer 4.1. Study period: April 2006–March 2007.

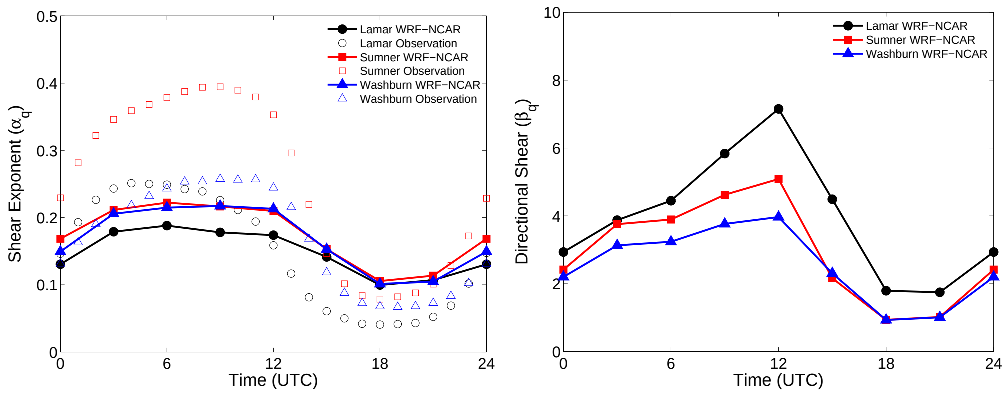

4.3. Spatial Distribution of Wind Shear Values over the USGP

Even though we have now established that the WRF model makes some errors in capturing annual average shear exponents, there are many benefits in using the WRF model forecasts for wind resource studies. One important advantage being the capability to estimate the shear exponents at every locations inside the computational domain (Figure 8). Figures 8 and 9 reveal that there are relationships between the shear exponent and land use, as well as terrain. The "hot spots" of high shear exponents are associated with larger cities, such as Oklahoma City, OK; Wichita, KS; and the Dallas-Fort Worth area in TX. These urban areas have large roughness lengths, which slow down the lowest level wind speeds. The higher model heights will not be as affected by the surface roughness, leading to a high shear exponent. Similarly, the region dominated by trees in eastern Oklahoma and Texas have large roughness lengths, causing the shear exponent to be large. Elevation also appears to have an effect on the shear exponent and directional shear, as higher values of directional shear, and low magnitude values of shear exponents, are located over the higher terrain to the west. There are also locations where local topography may have an impact on both the shear exponents and directional shear.

4.4. Sensitivity Studies

Up to this point, most of our analyses were based on the operational WRF-NCAR model forecasts, which utilized the YSU PBL scheme and the Eta/NAM (AWIP) data for initial and boundary conditions. In this sub-section, we would like to find out if the model-forecast derived shear exponents are sensitive to the PBL schemes and the initial-boundary data. Since it is computationally prohibitive to run a year worh of simulations using different PBL schemes and initial-boundary data, we focused on a two weeks period (May 19, 2006–May 31, 2006). The details of the simulations were discussed earlier in Section 3.2. The results are shown in Figure 10.

Figure 8. The WRF-NCAR model forecast-derived one-year average shear exponents (left panel) and magnitude of directional shear (right panel). Stars indicate location of tower locations used by SE06. Study period: April 2006–March 2007.

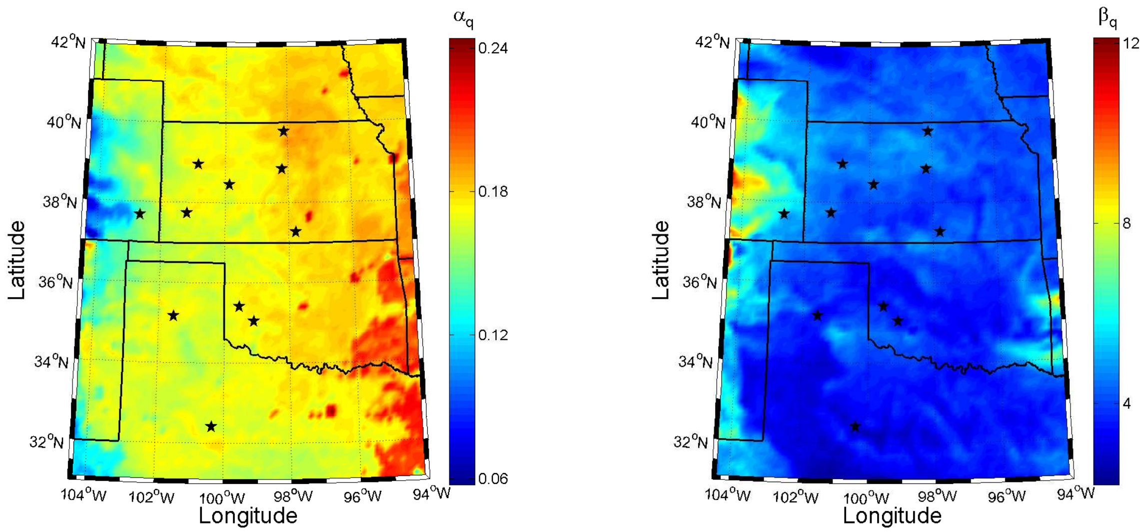

Figure 9. The WRF-NCAR model's terrain elevation (left panel) above mean sea level (m) and USGS land use (LU) categories that the WRF model assigns to the grid points (right panel). The LU indices are [39]: 1 – urban, 2 – dryland crop and pasture, 3 – irrigated crop and pasture, 5 – cropland/grass mosaic, 6 – cropland/wood mosaic, 7 – grassland, 8 – shrubland, 10 – savanna, 11 – deciduous broadleaf, 14 – evergreen needle-leat, 15 – mixed forest, and 16 – water bodies.

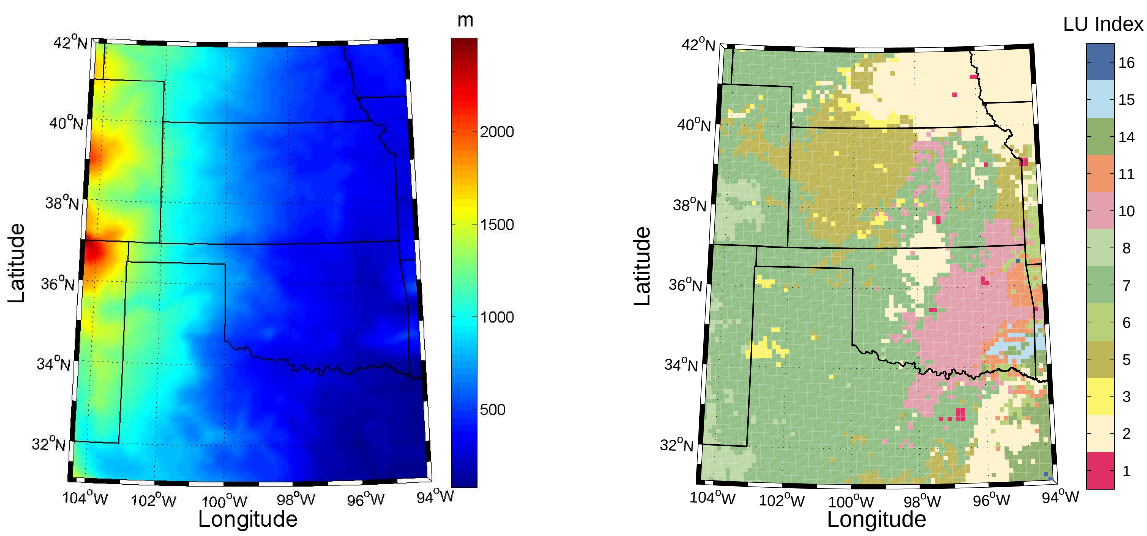

Figure 10. Diurnal variation of the observed and the WRF model forecast-derived wind shear exponents (left panel) and the directional shear magnitudes (right panel) at Sweetwater, TX. Study period: May 19, 2006–May 31, 2006.

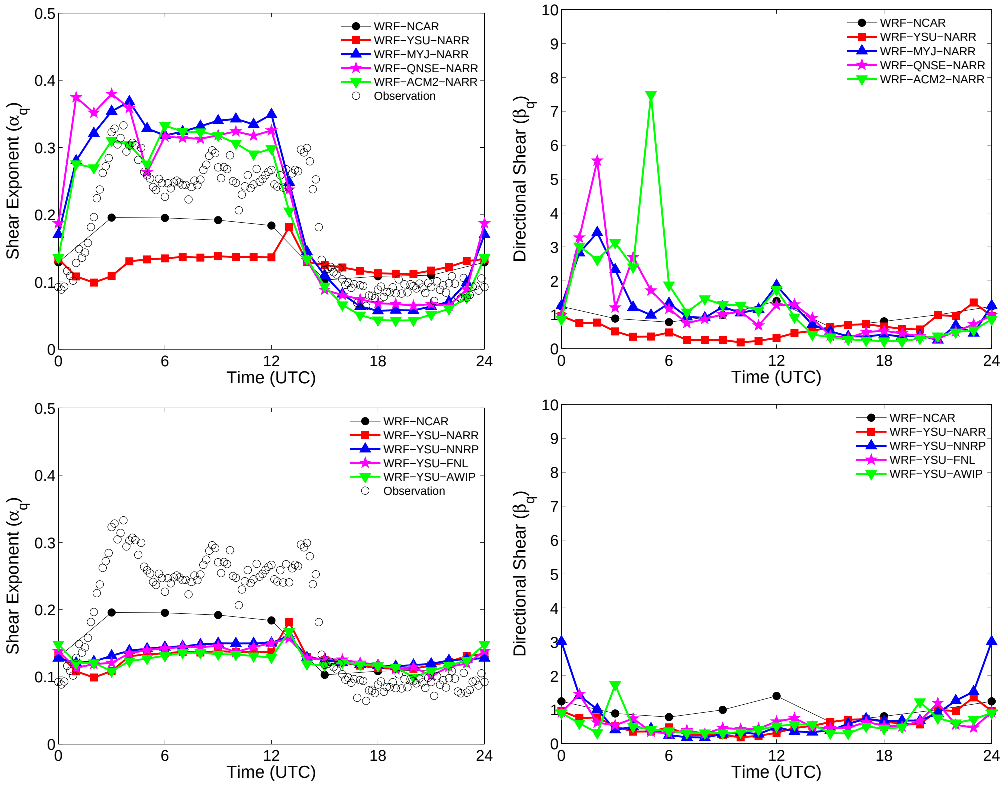

Based on Figure 10, we conclude:

- The model forecast-derived shear exponents are significantly more sensitive to the PBL schemes than the initial-boundary data;
- All the model runs capture the daytime wind speed shear exponents quite well;
- The model runs using the MYJ, QNSE, and ACM2 PBL schemes significantly overestimates the nighttime wind speed shear exponents;
- The model runs using the YSU PBL scheme severely underestimates the nighttime wind speed shear exponents;
- The model runs using the MYJ, QNSE, and ACM2 PBL schemes produce significantly higher directional shear during nighttime hours in comparison to the runs based on the YSU scheme.

The differences in estimated nighttime wind speed shear exponents between the WRF-NCAR and WRF-YSU-AWIP demand explanations. Both runs use the YSU PBL scheme and Eta/NAM (AWIP) data for initial and boundary conditions. However, the WRF-NCAR run used the version 2.1/2.2 of WRF, whereas the WRF-YSU-AWIP used the latest version 3.1.1. In the version 3.1.1., the YSU PBL scheme has been modified to provide enhanced diffusion during stably stratified (nighttime) conditions [40].

This modification has essentially lead to excessive mixing of the stable boundary layer and, in turn, has destroyed near-surface shear.

5. Concluding Remarks

In this paper, the WRF model was evaluated to determine if it can accurately represent site specific low-level wind shear, which is important for wind resource assessments as well as for turbine load estimations. By comparing one-year average shear exponent values from the WRF-NCAR model forecasts to the observational data, we found that the WRF-NCAR model forecasts, which utilized the YSU PBL scheme, overestimates the shear exponents during the daytime hours, and underestimates the shear exponents during the nighttime hours. Though no direct comparison between the WRF-NCAR model's directional shear magnitude and observations were feasible, our results indicate that there may be enough directional shear over the USGP to justify its inclusion in the future wind turbine design codes.

By conducting several sensitivity studies, we found that the estimated wind shear exponents are strongly dependent on the PBL scheme used. The effects of initial and boundary data on the estimation of the wind shear exponents were found to be minimal. Based on these findings, we recommend that the wind industry conduct multi-physics ensemble forecasts in future wind resource estimation projects to enhance the reliability of the low-level wind shear estimates.

Acknowledgements

This work was partially supported by the National Science Foundation (ATM-0748606, DGE-0221688) and the Texas Advanced Research Program (003658-0100-2007) grants. The authors are grateful to the National Center for Atmospheric Research for making the operational WRF forecasts available for this research. Special thanks go to David Carr for sending us the tall-tower data from Sweetwater, TX. The authors would also like to thank Dennis Elliott and Marc Schwartz for sharing information regarding their tall-tower related research works. We greatly acknowledge the valuable comments and suggestions made by Jimy Dudhia during the course of this study. All computational resources were kindly provided by the High Performance Computing Center at Texas Tech University.

References and Notes

1. AWEA Homepage. Available online: http://www.awea.org (accessed 10 February 2010).
2. Bonner, W.D. Climatology of the low-level jet. *Mon. Wea. Rev.* **1968**, *96*, 833–850.
3. Mitchell, M.J.; Arritt, R.W.; Labas, K. A climatology of the warm season Great Plains low-level jet using wind profiler observations. *Wea. Forecast.* **1995**, *10*, 576–591.
4. Whiteman, C.D.; Bian, X.; Zhong, S. Low-level jet climatology from enhanced rawinsonde observations at a site in the Southern Great Plains. *J. Appl. Meteorol.* **1997**, *36*, 1363–1376.
5. Song, J.; Liao, K.; Coulter, R.L.; Lesht, B.M. Climatology of the low-level jet at the Southern Great Plains atmospheric boundary layer experiments site. *J. Appl. Meteorol.* **2005**, *44*, 1593–1606.
6. Blackadar, K. Boundary layer wind maxima and their significance for the growth of nocturnal inversions. *Bull. Amer. Meteorol. Soc.* **1957**, *38*, 283–290.

7. Holton, J.R. The diurnal boundary layer wind oscillation above sloping terrain. *Tellus* **1967**, *19*, 199–205.
8. Reiter, E.R. *Jet Stream Meteorology*; University of Chicago Press: Chicago, IL, USA, 1963.
9. Kelley, N.; Shirazi, M.; Jager, D.; Wilde, S.; Adams, J.; Buhl, M.; Sullivan, P.; Patton, E. *Lamar Low-Level Jet Project Interim Report*; NREL/TP-500-34593; National Renewable Energy Laboratory: Golden, CO, USA, 2004.
10. *Wind Turbine Generator System Part 1: Design Requirements*, 3rd ed.; IEC 61400-1; International Electrotechnical Commission: Geneva, Switzerland, 2005.
11. Kelley, N.D.; Jonkman, B.J.; Scott, G.N. *The Great Plains Turbulence Environment: Its Origins, Impact and Simulation*; NREL/CP-500-40176; National Renewable Energy Laboratory, Golden, CO, USA, 2006.
12. Hand, M.M. *Mitigation of Wind Turbine/Vortex Interaction Using Disturbance Accomodating Control*; NREL/TP-500-35172; National Renewable Energy Laboratory: Golden, CO, USA, 2003.
13. Smith, K.; Randall, G.; Malcolm, D.; Kelley, N.; Smith, B. Evaluation of wind shear patterns at Midwest wind energy facilities. In *Proceedings of the American Wind Energy Association (AWEA) Windpower 2002 Conference*, Portland, OR, USA, June 2002.
14. Holtslag, A.A.M. Estimates of diabatic wind speed profiles from near-surface weather observations. *Boundary-Layer Meteorol.* **1984**, *29*, 225–250.
15. Giebel, G.; Gryning, S.E. *Shear and Stability in High Met Masts, and How WAsP Treats It*; Risϕ National Laboratory: Roskilde, Denmark, 2004.
16. Skamarock, W.C.; Klemp, J.B.; Dudhia, J.; Gill, D.O.; Barker, D.M.; Wang, W.; Powers, J.G. *Description of the Advanced Research WRF Version 2*; NCAR/TN-468+STR; National Center for Atmospheric Research: Boulder, CO, USA, 2005.
17. Schlichting, H. *Boundary-layer theory*, 6th ed.; McGraw-Hill: New York, NY, USA, 1968.
18. Arya, S.P. *Air Pollution Meteorology and Dispersion*; Oxford University Press: Oxford, UK, 1999.
19. Frost, R. The velocity profile in the lowest 400 feet. *Meteorol. Mag.* **1947**, *76*, 14–17.
20. Sisterson, D.L.; Frenzen, P. Nocturnal boundary-layer wind maxima and the problem of wind power assessment. *Environ. Sci. Tech.* **1978**, *12*, 218–221.
21. Irwin, J. A theoretical variation of the wind profile power-law exponent as a function of surface roughness and stability. *Atmos. Environ.* **1979**, *13*, 191–194.
22. Schwartz, M.; Elliot, D. Wind shear characteristics at central plains tall towers. In *Proceedings of the American Wind Energy Association (AWEA) Windpower 2006 Conference*, Pittsburg, PA, USA, 2006.
23. van Ulden, A.P.; Holtslag, A.A.M. Estimation of atmospheric boundary layer parameters for diffusion applications. *J. Clim. Appl. Meteorol.* **1985**, *24*, 1196–1207.
24. Hong, S.-Y.; Dudhia, J.; Chen, S.-H. A revised approach to ice-microphysical processes for the bulk parameterization of cloud and precipitation. *Mon. Wea. Rev.* **2004**, *132*, 103–120.
25. Mlawer, E.J.; Taubman, S.J.; Brown, P.D.; Iacono, M.J.; Clough, S.A. Radiative transfer for inhomogeneous atmospheres: RRTM, a validated correlated-k model for the longwave. *J. Geophys. Res.* **1997**, *102*, 16663–16682.

26. Dudhia, J. Numerical study of convection observed during the winter monsoon experiment using a mesoscale two-dimensional model. *J. Atmos. Sci.* **1989**, *46*, 3077–3107.
27. Hong, S.-Y.; Noh, Y.; Dudhia, J. A new vertical diffusion package with an explicit treatment of entrainment processes. *Mon. Wea. Rev.* **2006**, *134*, 2318–2341.
28. Chen, F; Dudhia, J. Coupling an advanced land surface hydrology model with the Penn State - NCAR MM5 modeling system. Part I: Model implementation and sensitivity. *Mon. Wea. Rev.* **2001**, *129*, 569–585.
29. Kain, J.S.; Fritsch, J.M. Convective parameterization for mesoscale models: The Kain-Fritsch scheme. In *The Representation of Cumulus Convection in Numerical Models of the Atmosphere*, Emanuel, K., Raymond, D.J., Eds.; American Meteorological Society: Boston, MA, USA, 1993; pp. 165–170.
30. Kain, J.S. The Kain-Fritsch convective parameterization: An update. *J. Appl. Meteorol.* **2004**, *43*, 170–181.
31. Janjic, Z.I. *Nonsingular implementation of the Mellor-Yamada level 2.5 scheme in the NCEP Meso model*; Office Note #437; National Centers for Environmental Prediction: Camp Springs, MD, USA, 2001.
32. Sukoriansky, S.; Galperin, B.; Perov, V. A quasi-normal scale elimination model of turbulence and its application to stably stratified flows. *Nonlinear Process. Geophys.* **2006**, *13*, 9–22.
33. Pleim, J.E. A combined local and nonlocal closure model for the atmospheric boundary layer. Part I: Model description and testing. *J. Appl. Meteorol. Clim.* **2007**, *46*, 1383–1395.
34. Tjernström, M.; Zagar, M.; Svensson, G.; Cassano, J.J.; Pfeifer, S.; Rinke, A.; Wyser, K.; Dethloff, K.; Jones, C.; Semmler, T.; Shaw, M. Modelling the arctic boundary layer: An evaluation of six ARCMIP regional-scale models using data from the SHEBA project. *Boundary-Layer Meteorol.* **2004**, *117*, 337–381.
35. Mathew, S. *Wind Energy: Fundamentals, Resource Analysis and Economics*; Springer: Berlin, Germany, 2006.
36. Beljaars, A.; Viterbo, P. The role of the boundary layer in a numerical weather prediction model. In *Clear and Cloudy Boundary Layers*, Holtslag, A.A.M., Duynkerke, P.G., Eds.; Royal Netherlands Academy of Arts and Sciences: Amsterdam, The Netherlands, 1998; pp. 297–304.
37. Viterbo, P.; Beljaars, A.; Mahfouf, J.-F.; Teixeira, J. The representation of soil moisture freezing and its impact on the stable boundary layer. *Quart. J. Royal Meteorol. Soc.* **1999**, *125*, 2401–2426.
38. Cuxart, J.; Holtslag, A.A.M.; Beare, R.J.; Bazile, E.; Beljaars, A.; Cheng, A.; Conangla, L.; Ek, M.; Freedman, F.; Hamdi, R.; Kerstein, A.; Kitagawa, H.; Lenderink, G.; Lewellen, D.; Mailhot, J.; Mauritsen, T.; Perov, V.; Schayes, G.; Steeneveld, G.-J.; Svensson, G.; Taylor, P.; Weng, W.; Wunsch, S.; Xu, K.-M. Single-column model intercomparison for a stably stratified atmospheric boundary layer. *Boundary-Layer Meteorol.* **2006**, *118*, 273–303.
39. Zehnder, J.A. Simple modifications to improve fifth-generation Pennsylvania State University-National Center for Atmospheric Research Mesoscale Model performance for the Phoenix, Arizona, metropolitan area *J. Appl. Meteorol.* **2002**, *41*, 971–979.

40. Hong, S.-Y.; Kim, S.-W. Stable Boundary Layer Mixing in a Vertical Diffusion Scheme. In *Proceedings of 9th WRF Users' Workshop*, Boulder, CO, USA, 2008.